Haploinsufficiency of the Chromatin Remodeler *BPTF* Causes Syndromic Developmental and Speech Delay, Postnatal Microcephaly, and Dysmorphic Features

Paweł Stankiewicz,[1,2,19,*] Tahir N. Khan,[3,19] Przemyslaw Szafranski,[1] Leah Slattery,[4] Haley Streff,[1] Francesco Vetrini,[2] Jonathan A. Bernstein,[4] Chester W. Brown,[5,6] Jill A. Rosenfeld,[1,2] Surya Rednam,[7,8,9] Sarah Scollon,[7,8,9] Katie L. Bergstrom,[7,8,9] Donald W. Parsons,[1,7,8,9] Sharon E. Plon,[1,7,8,9] Marta W. Vieira,[10] Caio R.D.C. Quaio,[11] Wagner A.R. Baratela,[11] Johanna C. Acosta Guio,[12] Ruth Armstrong,[13] Sarju G. Mehta,[13] Patrick Rump,[14] Rolph Pfundt,[15] Raymond Lewandowski,[16] Erica M. Fernandes,[16] Deepali N. Shinde,[17] Sha Tang,[17] Juliane Hoyer,[18] Christiane Zweier,[18] André Reis,[18] Carlos A. Bacino,[1,2] Rui Xiao,[1,2] Amy M. Breman,[1,2] Janice L. Smith,[1,2] Deciphering Developmental Disorders Study, Nicholas Katsanis,[3] Bret Bostwick,[1] Bernt Popp,[18] Erica E. Davis,[3,19] and Yaping Yang[1,2,19,*]

Bromodomain PHD finger transcription factor (BPTF) is the largest subunit of nucleosome remodeling factor (NURF), a member of the ISWI chromatin-remodeling complex. However, the clinical consequences of disruption of this complex remain largely uncharacterized. BPTF is required for anterior-posterior axis formation of the mouse embryo and was shown to promote posterior neuroectodermal fate by enhancing Smad2-activated *wnt8* expression in zebrafish. Here, we report eight loss-of-function and two missense variants (eight *de novo* and two of unknown origin) in *BPTF* on 17q24.2. The *BPTF* variants were found in unrelated individuals aged between 2.1 and 13 years, who manifest variable degrees of developmental delay/intellectual disability (10/10), speech delay (10/10), postnatal microcephaly (7/9), and dysmorphic features (9/10). Using CRISPR-Cas9 genome editing of *bptf* in zebrafish to induce a loss of gene function, we observed a significant reduction in head size of F0 mutants compared to control larvae. Terminal deoxynucleotidyl transferase dUTP nick end labeling (TUNEL) and phospho-histone H3 (PH3) staining to assess apoptosis and cell proliferation, respectively, showed a significant increase in cell death in F0 mutants compared to controls. Additionally, we observed a substantial increase of the ceratohyal angle of the craniofacial skeleton in *bptf* F0 mutants, indicating abnormal craniofacial patterning. Taken together, our data demonstrate the pathogenic role of *BPTF* haploinsufficiency in syndromic neurodevelopmental anomalies and extend the clinical spectrum of human disorders caused by ablation of chromatin remodeling complexes.

Introduction

Chromatin remodeling, an essential process regulating DNA accessibility and transcriptional activation, is controlled by covalent histone modifications and ATP-dependent nucleosome translocation which involves five conserved protein complexes: (1) SWI/SNF (a.k.a. BRG1-associated factors [BAF]), (2) ISWI (*imitation switch*), (3) CHD (chromatin helicase DNA-binding), (4) INO80/SWR1, and (5) ATRX.[1] Thus far, pathogenic variants in 11 chromatin remodeling genes involving SWI/SNF (BAF), CHD, and ATRX have been implicated in congenital disorders as well as cancer development, i.e., *ARID1A* (Coffin-Siris syndrome 2 [MIM: 614607]), *ARID1B* (Coffin-Siris syndrome 1 [MIM: 135900]), *SMARCA2* (Nicolaides-Baraitser syndrome [MIM: 601358]), *SMARCA4* (Coffin-Siris syndrome 4 [MIM: 614609] and Rhabdoid tumors [MIM: 613325]), *SMARCB1* (Coffin-Siris syndrome 3 [MIM: 614608], Rhabdoid tumors [MIM: 609322], and Schwannomatosis [MIM: 162091]), *SMARCD2* (specific granule deficiency 2 [MIM: 617475]), *SMARCE1* (Coffin-Siris syndrome 5 [MIM: 616938]), *CHD2* (epileptic encephalopathy, childhood-onset [MIM: 615369]), *CHD4* (Sifrim-Hitz-Weiss syndrome [MIM: 617159]), *CHD7* (CHARGE syndrome [MIM: 214800] and hypogonadotropic hypogonadism 5 with or without anosmia [MIM: 612370]), and *ATRX*

[1]Department of Molecular and Human Genetics, Baylor College of Medicine, Houston, TX 77030, USA; [2]Baylor Genetics, Houston, TX 77021, USA; [3]Center for Human Disease Modeling, Duke University Medical Center, Durham, NC 27701, USA; [4]Department of Pediatrics, Division of Medical Genetics, Stanford University, Stanford, CA 94305, USA; [5]University of Tennessee Health Science Center, Memphis, TN 38163, USA; [6]Le Bonheur Children's Hospital, Memphis, TN 38105, USA; [7]Texas Children's Hospital, Houston, TX 77030, USA; [8]Department of Pediatrics, Baylor College of Medicine, Houston, TX 77030, USA; [9]Texas Children's Cancer Center, Texas Children's Hospital, Houston, TX 77030, USA; [10]PUCSP, Faculdade de Ciências Médicas e da Saúde, São Paulo 01221-020, Brazil; [11]Fleury Medicina e Saúde, São Paulo 04344-070, Brazil; [12]Especialista en Genética Médica, Instituto de Ortopedia Infantil Roosevelt, 17-50 Bogotá, Cundinamarca, Colombia; [13]East Anglian Medical Genetics Service, Clinical Genetics, Addenbrooke's Treatment Centre, Addenbrooke's Hospital, Cambridge CB2 0QQ, UK; [14]Department of Genetics, University of Groningen, University Medical Center Groningen, 9700 AB Groningen, the Netherlands; [15]Department of Human Genetics, Radboud University Medical Center, 6500 HB Nijmegen, the Netherlands; [16]Virginia Commonwealth University, Richmond, VA 23298, USA; [17]Department of Clinical Genomics, Ambry Genetics, Aliso Viejo, CA 92656, USA; [18]Institute of Human Genetics, Friedrich-Alexander-Universität Erlangen-Nürnberg (FAU), Erlangen 91054, Germany
[19]These authors equally contributed to this work
*Correspondence: pawels@bcm.edu (P.S.), yapingy@bcm.edu (Y.Y.)
http://dx.doi.org/10.1016/j.ajhg.2017.08.014.

(alpha-thalassemia/mental retardation syndrome [MIM: 301040]). To date, neither INO80/SWR1 nor ISWI genes have been associated with disease in humans.

The ISWI family member NURF (nucleosome remodeling factor) is an evolutionarily conserved key transcriptional regulator of development[2] in a locus-specific manner[3,4] by virtue of the complex's chromatin remodeling activity.[5,6] In vertebrates, NURF consists of SNF2L (ISWI homolog encoded by *SMARCA1*), pRBAP46/48, and the largest subunit BPTF (bromodomain PHD finger transcription factor).[7–9] Human BPTF contains two PHD finger domains followed proximally by a bromodomain (BRD). The second PHD finger of BPTF mediates binding of the NURF complex to chromatin with trimethylation of histone H3 lysine 4 (H3K4me3).[10] In a combinatorial manner via multivalent interactions together with the PHD finger, the BRD binds to acetylated lysine 16 in histone H4 (H4K16ac), enabling the selective targeting of BPTF to chromatin that contains both histone marks, thereby increasing its selectivity.[11–14]

Heterozygous *Bptf* mutant mice are apparently normal and fertile with no obvious phenotype.[15] Analyses of homozygous mice have revealed that BPTF is essential for the formation of mesoderm, endoderm, and differentiated ectoderm lineages and is required for the establishment of the embryonal anterior-posterior axis during early development; homozygotes show lethality at embryonic day (E)7.5 to E8.5 with 100% penetrance.[16] BPTF was also found to be important for trophoblast differentiation during early mouse development (E6.5).[15] Additionally, depletion of *Bptf* has enhanced T cell-mediated antitumor immunity in two syngeneic mouse models of cancer.[17]

Consistent with murine mutant data, Bptf was shown previously to promote neuroectodermal posteriorization in zebrafish embryos. RNA *in situ* hybridization and protein analyses demonstrated that *bptf* is expressed ubiquitously during zebrafish early embryonic development, and it is expressed abundantly in the zebrafish head through 30 hr post fertilization (hpf).[18] Morpholino-based suppression of *bptf* results in abnormal anterior patterning and defects in neural posteriorization; these phenotypes are attributed to misregulated TGF-β/Smad2 signaling and concomitant restriction of *wnt8a* expression.[18] The TGF-β pathway is critical for cellular growth, differentiation, and apoptosis and was shown to be an important driver in neurogenesis and central nervous system development.[19] Moreover, zebrafish *wnt8a* was shown to function in early-stage mesoderm patterning and posteriorization of the neuroectoderm.[20]

In humans, BPTF is ubiquitously expressed.[10] Amplification and overexpression of *BPTF* were reported in a variety of cancers including breast, lung, and brain.[21–26] BPTF was shown as essential for T cell homeostasis and function.[27] BPTF also inhibits fNK cell activity and the abundance of natural cytotoxicity receptor co-ligands.[28] Lastly, BPTF maintains chromatin accessibility and the self-renewal capacity of mammary gland stem cells.[29]

Here, we describe phenotypic manifestations of germline loss-of-function (LoF) variants in *BPTF* in ten unrelated individuals with an autosomal-dominant neurodevelopmental disorder and show with an *in vivo* zebrafish model that *bptf* is relevant to brain development and craniofacial patterning.

Material and Methods

Subjects

The study cohort consists of ten unrelated case subjects. Individuals 1–3 were found in the exome database of 9,056 individuals referred for clinical whole-exome sequencing (WES) at Baylor Genetics (BG). Individuals 4 and 5 were identified in the clinical database of 75,795 subjects referred for clinical chromosomal microarray analysis (CMA) at BG. These five subjects were chosen through filtering for potentially LoF variants in previously unsolved case subjects with overlapping neurological phenotypes. Subsequently, we identified three additional individuals: via DECIPHER[30] individuals 6 (DECIPHER 275557) and 7 (DECIPHER 264215) from the Deciphering Developmental Disorders (DDD) Study cohort[31] and individual 8 from the University of Groningen, the Netherlands. Through the online matchmaker platform GeneMatcher,[32] individuals 9 and 10 were identified from the Institute of Human Genetics, Friedrich-Alexander-Universität Erlangen-Nürnberg in Erlangen, Germany and Virginia Commonwealth University in Richmond, respectively. Written informed consent (for individuals 1–3, 6–10) was obtained in accordance with protocols approved by the appropriate human subject ethics committees; individuals 4 and 5 were covered by a protocol (with waiver of consent) approved by Baylor College of Medicine. The study has UK Research Ethics Committee approval (10/H0305/83, granted by the Cambridge South REC, and GEN/284/12 granted by the Republic of Ireland REC).

Microarray and Molecular Analyses

Individuals 1–3 were analyzed at BG Laboratories by trio WES (individual 1) or proband-only WES (individuals 2 and 3) using the capture design based on VCRome by NimbleGen.[33] The mean coverage of target bases was >120×, and >96% target bases were covered at >20×. PCR amplification and Sanger sequencing to verify all candidate variants were done according to standard procedures in the proband and the parents when available, and candidate variants were annotated using the *BPTF* RefSeq transcript GenBank: NM_004459.6. The two copy-number variant (CNV) deletions in individuals 4 and 5 were detected at BG using customized exon-targeted oligo arrays (OLIGO V8.1.1 and V11.2),[34,35] which cover more than 1,700 and 4,800 disease-associated genes, respectively, with exon-level resolution. CNV deletion junction fragments were amplified using long-range PCR with LA Taq DNA polymerase (TaKaRa Bio) and primers designed by Primer3 software. Individuals 6 and 7 were recruited and analyzed by WES in the DDD Study.[31] The variant in individual 8 was detected in the Department of Human Genetics, Radboud University Medical Center, in Nijmegen, the Netherlands. The mutation in individual 9 was identified within an exome Pool-Seq screening approach which will be published elsewhere (B. Popp, unpublished data); validation and segregation analysis was performed by Sanger sequencing followed by genetic fingerprinting using the PowerPlex 21 system (Promega) to confirm

de novo occurrence. For individual 10, parent-proband trio WES was performed at Ambry Genetics using the IDT xGen Exome Research Panel and analyzed as previously described.[36,37] On average, ~96.6% of the target bases were covered at >20× for the trio. The *de novo* frameshift alteration identified in this patient by WES was confirmed by Sanger sequencing and interpreted as a (suspected) candidate gene finding.[37]

CRISPR-Cas9 Genome Editing

We identified a single zebrafish (*Danio rerio*) ortholog of *BPTF* using reciprocal BLAST (Ensembl ID: ENSDART00000109601; GRCz10; 51% similarity to human *BPTF*; Figure S1). The CRISPR single-guide (sgRNA) target was identified with ChopChop software[38] and synthesized using the GeneArt Precision gRNA Synthesis Kit (Invitrogen) according to manufacturer's instructions as described.[39] To generate F0 mutants, 75 pg of sgRNA and 150 pg of CAS9 protein (PNA bio, CP01) were injected directly into the cell of 1-cell stage zebrafish embryos. The efficiency of the sgRNA was determined by extracting genomic DNA from F0 embryos at 2 dpf by proteinase K digestion (Life technologies, AM2548). The sgRNA genome editing site was PCR amplified and resulting PCR products were denatured and slowly reannealed (denaturing at 95°C for 5 min, ramped down to 85°C at −1°C/s and then to 25°C at −0.1°C/s) to facilitate heteroduplex formation. Heteroduplexes were detected by 15% polyacrylamide gel electrophoresis[38] (n = 6 F0 embryos and 1 uninjected control embryo) followed by cloning and sequencing of PCR amplicons to estimate mosaicism.

Zebrafish Embryo Injections

Zebrafish embryos were collected from natural matings of *-1.4col1a1:egfp*[40] heterozygous adults. For CRISPR experiments, one-cell stage embryos were injected with 1 nL, with the investigator masked to injection cocktail. Embryos were maintained in fresh embryo media (0.3 g/L NaCl, 75 mg/L $CaSO_4$, 37.5 mg/L $NaHCO_3$, 0.003% methylene blue) at 28°C until phenotypic endpoints. Larvae were phenotyped for cell death and cell proliferation at 2 days post fertilization (dpf); and for head size and craniofacial patterning at 3 dpf.

Zebrafish Phenotyping

Whole-Mount TUNEL Assay

Apoptotic cell death was detected by the terminal deoxynucleotidyl transferase dUTP nick end labeling (TUNEL) assay as described.[41] Briefly, 2 dpf embryos were dechorionated and fixed in 4% paraformaldehyde (PFA) at 4°C overnight and then in 100% methanol at −20°C for 2 hr. After rehydration in PBS, embryos were permeabilized with proteinase K (10 μg/mL) and postfixed with 4% PFA. Embryos were incubated in equilibration buffer and then with TdT enzyme followed by anti-digoxigenin provided in ApopTag Red *In Situ* Apoptosis Detection Kit (Millipore) as suggested by the manufacturer. We imaged the dorsal anterior aspect of whole-mounts with Z stack image capture using a Nikon AZ100 fluorescent microscope. TUNEL stain was quantified by counting positive cells in defined regions of the head with ImageJ software.

Cell Proliferation Assay

At 2 dpf, embryos were dechorionated and fixed in Dent's solution overnight at 4°C. Embryos were rehydrated in PBS with a stepwise reduced concentration of methanol, and then bleached, postfixed with 4% PFA, and permeabilized using proteinase-K. Embryos were then washed twice in IF buffer (1% BSA, 0.1% Tween-20 in 1× PBS) and incubated overnight with anti-p-histone H3 (PH3; 1:500, Santa Cruz Biotechnology, sc-8656-R). Following two washes in IF buffer, embryos were placed in secondary antibody solution containing Alexa Fluor 488 goat anti-rabbit IgG (1:500; Invitrogen) in blocking solution for 1 hr at room temperature. Z stacked images were captured using a Nikon AZ100 fluorescent microscope. Immunostained cells in defined regions of the dorsal aspect of the head were counted with ImageJ software.

Automated Live Phenotyping of Larval Head Size and Craniofacial Patterning

We positioned and imaged live 3 dpf larvae with the Vertebrate Automated Screening Technology (VAST; software v.1.2.3.6) to capture dorsal (head size; bright field) or ventral (craniofacial skeleton; fluorescent excitation at 470 nm) images. Larvae were anesthetized, pattern recognition templates were created, and all VAST operational settings were similar to those described.[42] Once recognized inside the 600 μm borosilicate capillary, each larva was rotated to capture images using a 5× fluar objective and Axiocam 503 monochromatic camera (Zen Pro software; Zeiss). Head size and ceratohyal cartilage angle were measured in respective images using ImageJ software and pairwise comparisons to determine statistical significance were made via a Student's t test.

Results

Clinical Findings

We identified 10 unrelated individuals with unique apparent non-mosaic variants in *BPTF*. The affected individuals included six males and four females, aged 2.1 to 13 years at the last clinical assessment (Table 1, Figure 1A). Common features included developmental delay (DD)/intellectual disability (ID) (10/10), speech delay (10/10), microcephaly (7/9), motor delay (8/10), hypotonia (5/10), and dysmorphic features (9/10), which included prominent nose (7/10), up-slanting or short palpebral fissures (4/10), and flaring of eyebrows (2/10), 5th finger clinodactyly (3/10), and bulbous halluces/broad great toes/sandal foot (5/10) (Table 1). Of note, individual 3 had clinical WES as part of an NIH-supported pediatric cancer study due to a diagnosis of pheochromocytoma, and WES resulted in a *VHL* pathogenic heterozygous variant c.499C>T (p.Arg167Trp) (GenBank: NM_000551.3) (Table S1).[43] The medical record and WES requisition form had also noted mild developmental delay and speech delay.

Clinical CMA and WES

Exome sequencing identified four frameshifting indels affecting the coding exons (c.989del [p.Leu330Argfs*28], c.2744del [p.Asn915Thrfs*36], c.2860dup [p.Glu954Glyfs*5], and c.5216_5217del [p.Val1739Glyfs*96]); one splicing/frameshifting indel (c.3360_3370+1del), which is predicted to eliminate 11 nucleotides of the coding region plus the first nucleotide of the invariant splice donor site sequence (GT); one nonsense variant (c.8650A>T [p.Lys2884*]); and two missense variants (c.5770G>A [p.Ala1924Thr] and c.8558T>G [p.Met2853Arg]) (GenBank: NM_004459.6) (Figure 1B). In eight subjects, the variants arose *de novo*; the

Table 1. Clinical and Genetic Findings in Individuals with *BPTF* Variants

	Subject 1	Subject 2	Subject 3	Subject 4	Subject 5	Subject 6	Subject 7	Subject 8	Subject 9	Subject 10
Variant (GRCh37; GeneBank NM_004459.6)	chr17: g.65890220dup	chr17: g.65908838_ 65908839del	chr17: g.65972049A>T	chr17: g.65700188-65896330del (196 kb)	chr17: g.65898399-65986981del (89 kb)	chr17: g.65905867_ 65905878del	chr17: g.65914918G>A	chr17: g.65971957T>G	chr17: g.65850431del	chr17: g.65889796del
	c.2860dup	c.5216_5217del	c.8650A>T	c.-121653_ 2922-3575del	c.2922-1506_ *8577del	c.3360_ 3370+1del	c.5770G>A	c.8558T>G	c.989del	c.2744del
	p.Glu954Glyfs*5	p.Val1739Glyfs*96	p.Lys2884*	CNV deletion	CNV deletion	r.spl?	p.Ala1924Thr	p.Met2853Arg	p.Leu330Argfs*28	p.Asn915Thrfs*36
Exon	9	13	29	1–9	10–30	12	14	29	2	8
Variant type	frameshift	frameshift	nonsense	CNV deletion	CNV deletion	splicing & frameshift	missense	missense	frameshift	frameshift
Variant inheritance	*de novo*	mother negative, father unavailable	*de novo*	*de novo*	unknown	*de novo*	*de novo*	*de novo*	*de novo*	*de novo*
Ethnicity	white	Latino	Latino	Latino	Latino	white	white	white	white	white
Gender	M	M	M	F	F	M	M	F	M	F
Age at last assessment (years)	2.1	7.9	10.9	10	4.3	13	11	11	7.11	12
Weight at birth (kg) (Z score)	2.7 (Z = −1.42)	2.63 (Z = −0.8)	ND	3.4 (Z = 0.00)	2.4 (Z = −3.6)	4.39 (Z = 0.84)	1.89 (Z = −3.44)	2.27 (Z = −3.5)	3.46 (Z = −0.06)	2.69 (Z = −1.38)
Length at birth (cm) (Z score)	ND	47 (Z = −0.7)	ND	50 (Z = 0.28)	48 (Z = −3.82)	ND	ND	45 (Z = −3.8)	51 (Z = −0.39)	48.3 (Z = 0.46)
Head circumference at birth (cm) (Z score)	33 (Z = −1.13)	33 (Z = −0.3)	ND	33 (Z = −1.11)	ND	36 (Z = 0.11)	33 (Z = −1.17)	ND	34.5 (Z = −0.62)	33 (Z = −0.74)
Weight at assessment (kg) (Z score)	10.1 (Z = −2.29)	20.6 (Z = −1.58)	30.1 (Z = −0.98)	37.8 (Z = 0.65)	17 (Z = 0,13)	22.3 (Z = −1.83)	23.2 (Z = −2.85)	25.5 (Z = −2.68)	19.5 (Z = −2.09)	26.05 (Z = −3.53)
Height at assessment (cm) (Z score)	84.5 (Z = −0.85)	117.1 (Z = −1.85)	142.2 (Z = −0.15)	143 (Z = 0.70)	88 (Z = −3.93)	134 (Z = 0.01)	126 (Z = −2.83)	137 (Z = −2.30)	120 (Z = −1.35)	134.4 (Z = −3.03)
Head circumference at assessment (cm) (Z score)	45 (Z = −2.05)	49.2 (Z = −2.1)	ND	51 (Z = −1.04)	46 (Z = −2.48)	50.2 (Z = −2.52)	54.2 (Z = −0.35)	49 (Z = −2.68)	48.3 (Z = −2.90)	49.5 (Z = −2.05)

(*Continued on next page*)

Table 1. ***Continued***

	Subject 1	Subject 2	Subject 3	Subject 4	Subject 5	Subject 6	Subject 7	Subject 8	Subject 9	Subject 10
Developmental delay/intellectual disability	mild	severe	mild	moderate	mild autistic spectrum disorder	moderate autistic spectrum disorder	severe	mild	moderate aggression and distractedness, disturbed sleep rhythm and sleeping problems	mild
Speech/language delay	+	+	+	+	+	+	+	+	+	+
Motor delay	+	+	+	+	–	–	+	+	+	–
Hypotonia	+	–	–	+	–	–	+	–	+	+
Microcephaly	+	+	ND	–	+	+	–	+	+	+
Brain anomalies	small anterior pituitary	ND	ND	brain MRI: bilateral nonspecific multifocal white matter lesions	–	ND	pituitary hypoplasia	brain MRI: reduced signal intensity of frontal and temporal white matter	MRI at age 4 years 8 months: periventricular white matter lesions	MRI brain: borderline low positioned cerebellar tonsil on right; no true Chiari
Dysmorphism	–	multiple lateral flaring of eyebrows, bilateral occipital protuberances, long nasal bridge with mildly hypolastic alae nasi	large helices of both ears (similar to father)	ocular hypertelorism, epicantal folds, up-slanting palpebral fissures, prominent nose	up-slanting palpebral fissures, hypertelorism, mediofacial hypoplasia	high palate, prominent nose and columella, thin upper lip	lateral flaring of eyebrows, prominent supraorbital ridges, short palpebral fissures, broad nasal tip, prominent gum line, Peg like, disorganized teeth	short palpebral fissures, long nose, mildly hypolastic alae nasi, full lower lip, prominent ears, micrognathia	long nasal bridge, small mouth and micrognathia	telecanthus, prominent nasal root with mildly bulbous nasal tip, micrognathia
Ophthalmological anomalies	–	outward deviation of one eye	–	–	–	–	severe myopia and convergent squint	–	cataract in right eye, hyperopia	myopia
Skeletal abnormalities	–	pes planus, 5th digit clinodactyly, windswept 2nd toe with lateral deviation, broad short great toes	–	advanced bone age	5th digit clinodactyly	slender fingers and toes, bulbous halluces	wrinkly hands, flexed fingers, 5th finger clinodactyly, bulbous halluces, overlapping toes	broad halluces, premature eruption of permanent mandibular central incisors	sandal gap of both feet	congenital hip dysplasia, small hands

Abbreviations: MRI, magnetic resonance imaging; ND, not determined because of non-availability or non-applicability

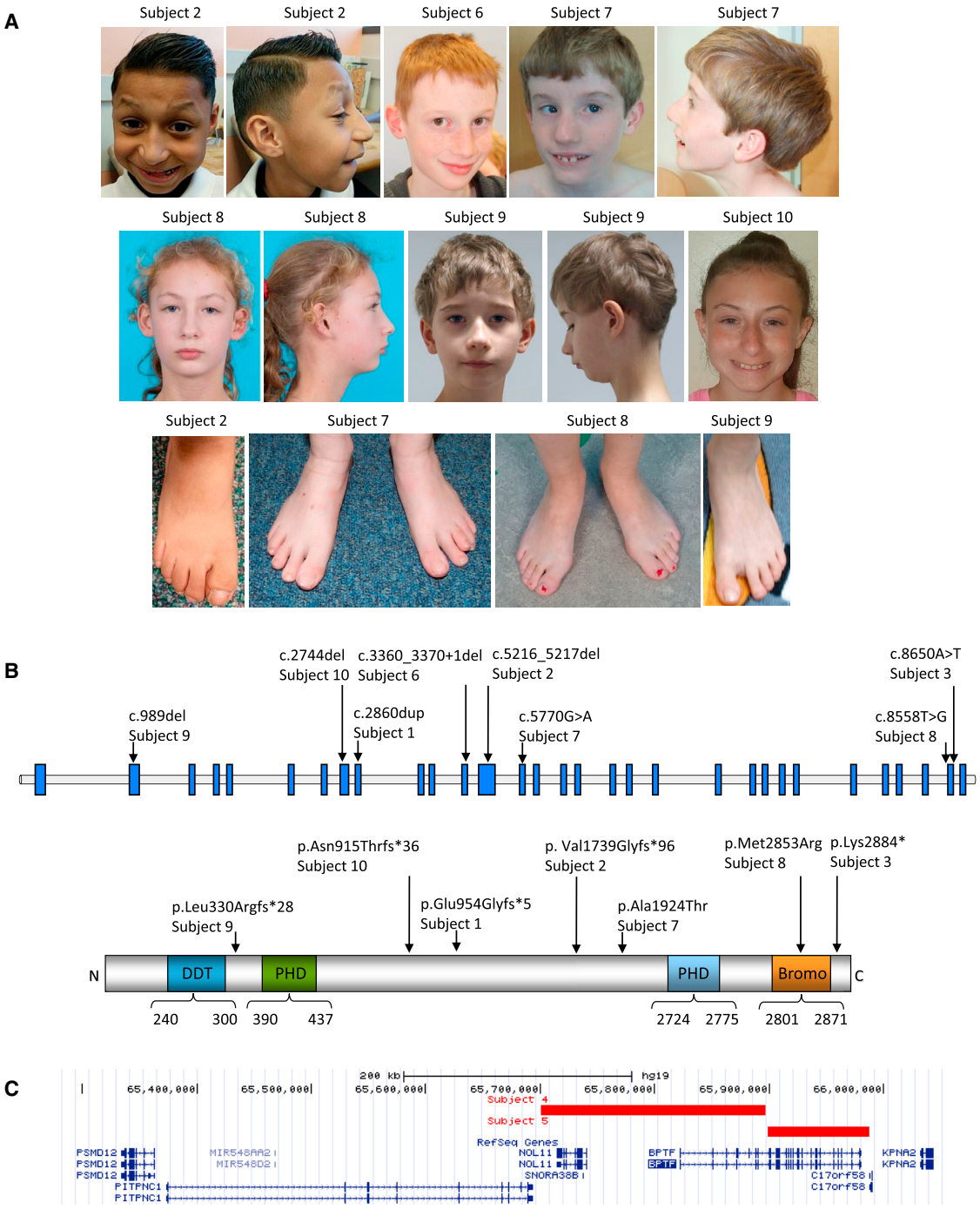

Figure 1. Clinical and Genetic Findings of Individuals with BPTF Variants

(A) Clinical features of subjects 2 and 6–10. Note the lateral flaring of eyebrows, long nasal bridge, windswept 2nd toe with lateral deviation, and broad short great toe in subject 2; prominent nose and columella and thin upper lip and in subject 6; prominent supraorbital ridges, lateral flaring of eyebrows, short palpebral fissures, convergent squint, broad nasal tip, disorganized teeth, bulbous halluces, and overlapping toes in subject 7; short palpebral fissures, long nose, prominent ears, mildly hypolastic alae nasi full lower lip, micrognathia, and broad halluces in subject 8; long nasal bridge, small mouth, micrognathia, and sandal gap in subject 9; and telecanthus, prominent nasal root with mildly bulbous nasal tip, and micrognathia in subject 10.

(B) A schematic of *BPTF*, the protein, and the effects of variants identified in this study. Domains represented in colors are: different transcription factors domain (DDT), PHD finger domain (PHD), and bromodomain (Bromo). The domain structure and amino acid numbering is based on the NCBI reference sequences GenBank: NP_003482.3 and NP_00450.3.

(C) A schematic of chromosomal region 17q24.2 showing the deletions affecting *BPTF* in the UCSC browser.

origin of the other two changes could not be determined (Table 1). The eight truncating variants are predicted to result in haploinsufficiency of the gene. The two *de novo* missense variants, c.5770G>A (p.Ala1924Thr) and c.8558T>G (p.Met2853Arg), are predicted to be likely damaging by most of the in silico prediction programs, including

PolyPhen-2 and MutationTaster (Table S2). Human splicing finder also reported the generation of a cryptic acceptor site for the variant c.8558T>G, although MaxEntScan and SPIDEX did not find a significant splice alteration. The two variants are not present in the Genome Aggregation Database (gnomAD) database (>122,000 individuals; accessed on 6/18/2017). In addition, Met2853 is located in the bromodomain; 3D simulation based on crystal structure of PHD finger-linker-bromodomain fragment of human BPTF (PDB: 3UV2) indicates that the substitution of Met with the positively charged Arg in the hydrophobic core may destabilize the 3D conformation of the BRD (Figure S2). Our collective data indicate that the missense variants likely disrupt the protein function.

CMA using V11.2 array in subject 4 revealed an ~157 kb CNV deletion on chromosome 17q24.2 (65,720,270–65,877,348, GRCh37/hg19), involving *BPTF*, and a ~1 kb CNV deletion of unknown significance on chromosome 14q11.2 (21,681,066-21,682,235), involving a non-disease-associated gene *HNRNPC*. CMA of the parental samples showed no evidence of these deletions. CMA using V8.1.1 array in subject 5 showed an ~63 kb CNV deletion on chromosome 17q24.2 (65,909,023–65,972,166), involving *BPTF* and a likely benign ~703 kb CNV duplication on chromosome 2q12.3 (108,403,193–109,106,402). Parental samples were not available. DNA sequencing of the junction fragment in subject 4 mapped the proximal breakpoint within *Alu*Sx between chr17: 65,700,189 and 65,700,200 and the distal breakpoint within *Alu*Sz6 between chr17: 65,896,331 and 65,896,342 with 12 bp microhomology, eliminating the 5′ end of the gene through exon 9. PCR analyses showed no evidence of low-level somatic mosaicism for the copy-number loss on 17q24.2 in either parent. In subject 5, the proximal deletion breakpoint was mapped within a unique sequence between chr17: 65,898,399 and 65,898,404 and the distal breakpoint within *Alu*Sp between 65,986,981 and 65,986,986 with a 4 bp GTGA microhomology, eliminating exon 10 through the 3′ end of the gene (Figures 1C and S3).

CRISPR/CAS9 Genome Editing of *bptf* in Zebrafish Results in Head Size Reduction Likely Caused by an Increase in Neuronal Cell Death

Although suppression of *bptf* implicated discrete morphogenetic pathways in aberrant neural patterning,[18] the eventual effects on zebrafish head size or craniofacial structures were unexplored previously in transient *bptf* knockdown models. To determine the relevance of *BPTF* disruption to patient phenotype, we used CRISPR-CAS9 to generate a *bptf* LoF model. We and others have shown previously that neuroanatomical defects can be modeled in zebrafish as a direct readout for analogous defects observed in humans.[31,44–47] We designed a CRISPR single-guide RNA (sgRNA) targeting exon 9 of *bptf*, injected 75 pg sgRNA and 150 pg of CAS9 into the cell of 1-cell-stage zebrafish embryos, and detected efficient disruption of the locus through the introduction of small insertions or deletions (90% mosaicism; Figure S1, Table S3). First, we asked whether we could detect any differences in the head size of 3 dpf F0 mutant larvae. We observed a significant reduction in a defined region of the head of *bptf* CRISPR F0 mutants compared to either control larvae or compared to larval batches injected with sgRNA alone (without CAS9); ($p \leq 0.0001$, n = 26–52 larvae/batch, repeated, Figure 2). To determine the cellular basis of this head size reduction in *bptf* F0 mutants, we performed TUNEL staining and PH3 staining to assess cell death and cell proliferation, respectively. We observed a significant increase in cell death in F0 mutants compared to control larvae and larvae injected with sgRNA alone ($p = 0.0004$ versus control, $p = 0.0003$ versus sgRNA alone, n = 20 larvae per condition, repeated). However, we did not detect any significant differences in cell proliferation between *bptf* F0 CRISPR mutants and controls (Figure 2).

bptf F0 Mutants Display Abnormal Craniofacial Patterning

To determine the relevance of *BPTF* ablation to the dysmorphic features observed in our cohort and to assess the role of *BPTF* in craniofacial patterning, we injected *bptf* sgRNA and CAS9 in *-1.4col1a1:egfp* transgenic embryos and assessed cartilage structures. We and others have shown that zebrafish can serve as robust direct models for craniofacial abnormalities observed in humans.[39,42,48–52] We assessed the craniofacial patterning by measuring the angle of ceratohyal (CH) cartilage in ventral images acquired from 3 dpf larvae. We observed a significant increase of the CH angle in *bptf* CRISPR F0 mutants (102° versus 91° for F0 mutants versus controls; $p \leq 0.0001$, n = 47–59 larvae/batch, repeated; Figure 2). Importantly, injection of *bptf* sgRNA alone was indistinguishable from that of controls, excluding the possibility of sgRNA toxicity inducing phenotypic differences.

Discussion

Here, we describe syndromic anomalies in ten individuals with potentially deleterious variants in *BPTF*, which encodes the largest subunit of the ATP-dependent chromatin-remodeling ISWI family member NURF. We identified five small frameshift indels, one nonsense variant, two missense variants, and two CNV deletions. For all affected individuals (n = 8) whose parents were both studied, the *BPTF* variant occurred *de novo*. *BPTF* is predicted to be highly intolerant to LoF mutations (probability of LoF intolerance, pLI = 1.0 in ExAC, accessed 6/18/2017).[53] Our data indicate that the most likely pathomechanism of *BPTF* is haploinsufficiency. All individuals in this study had variants that affect *BPTF* only, with the exception of individual 4, who carried a deletion that affects *BPTF* and *NOL11*. However, the low pLI score for *NOL11* (pLI = 0.03) suggests that disruptions of this gene are

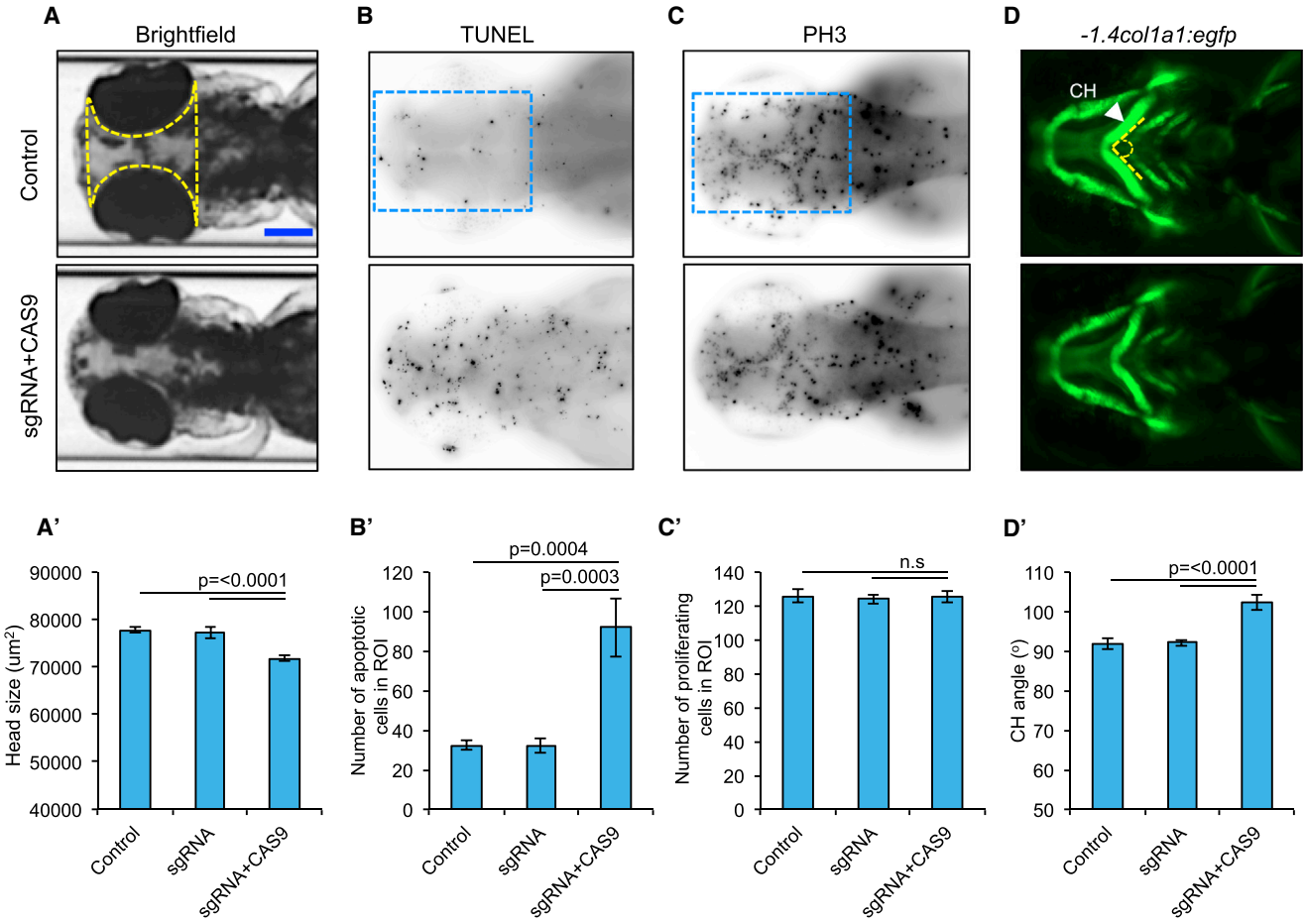

Figure 2. *bptf* CRISPR F0 Mutants Exhibit Microcephaly, Apoptosis in Anterior Structures, and Aberrant Patterning of the Branchial Arches

(A) Representative dorsal images of 3 dpf zebrafish larvae show a reduction in head size (yellow dotted area) in F0 mutants. Scale bar (blue), 150 μm.

(A′) Quantification of head size area in *bptf* F0 mutants ($p \leq 0.0001$ versus control, n = 26–52 larvae/batch, repeated). Solid yellow line indicates scale bar.

(B) Representative dorsal images of 2 dpf zebrafish larvae display increased apoptosis in the forebrain-midbrain region (blue dotted rectangle).

(B′) Apoptotic cell count in *bptf* CRISPR F0 mutants ($p = 0.0004$ versus control, n = 20 larvae/condition per batch, repeated).

(C) Representative dorsal images of 2 dpf zebrafish larvae do not show cell proliferation defects in anterior structures (blue dotted rectangle).

(C′) Cell proliferation count in *bptf* CRISPR F0 mutants (n.s., no statistical significance, n = 20 larvae/condition per batch).

(D) Representative ventral views of *-1.4col1a1:egfp* larvae imaged live at 3 dpf show an increase in the ceratohyal cartilage (CH; arrowhead) angle (dotted line) in F0 mutants.

(D′) Quantification of the ceratohyal angle in *bptf* F0 CRISPR mutants ($p \leq 0.0001$, n = 47–59 larvae/batch, repeated). Error bars indicate standard error of the mean (SEM).

unlikely to cause an autosomal-dominant disorder (Figure 3). These data are supported further by the observation that zebrafish F0 mutants with depleted *bptf* display relevant neuroanatomical and craniofacial defects. However, further studies in stable *bptf* mutants will be required to correlate precisely gene dosage with phenotype in this model system.

In addition to the variable degree of DD/ID and speech delay present in all reported subjects studied, the most consistent finding is postnatal microcephaly,[54] observed in 7/9 subjects. Interestingly, dysfunction of five genes reported previously to cause chromatin remodeling disorders are associated with microcephaly (*SMARCA2*, *SMARCA4*, *SMARCB1*, *SMARCE1*, and *CHD7*) and one is associated with macrocephaly (*CHD4*), suggesting that disruption of chromatin remodeling can have global consequences on brain development likely by deregulating multiple transcription factors. Unlike primary microcephaly, usually caused by a decrease in the number of neurons generated during neurogenesis, secondary microcephaly is thought to result from the postnatal reduction of dendritic processes, myelination, and synaptic connections.[55] Corroboratively, our studies of *bptf* deficiency in zebrafish showed a significant increase in neuronal cell death.

Reduction in brain volume found in microcephalic individuals is often associated with brain anomalies, DD/ID,

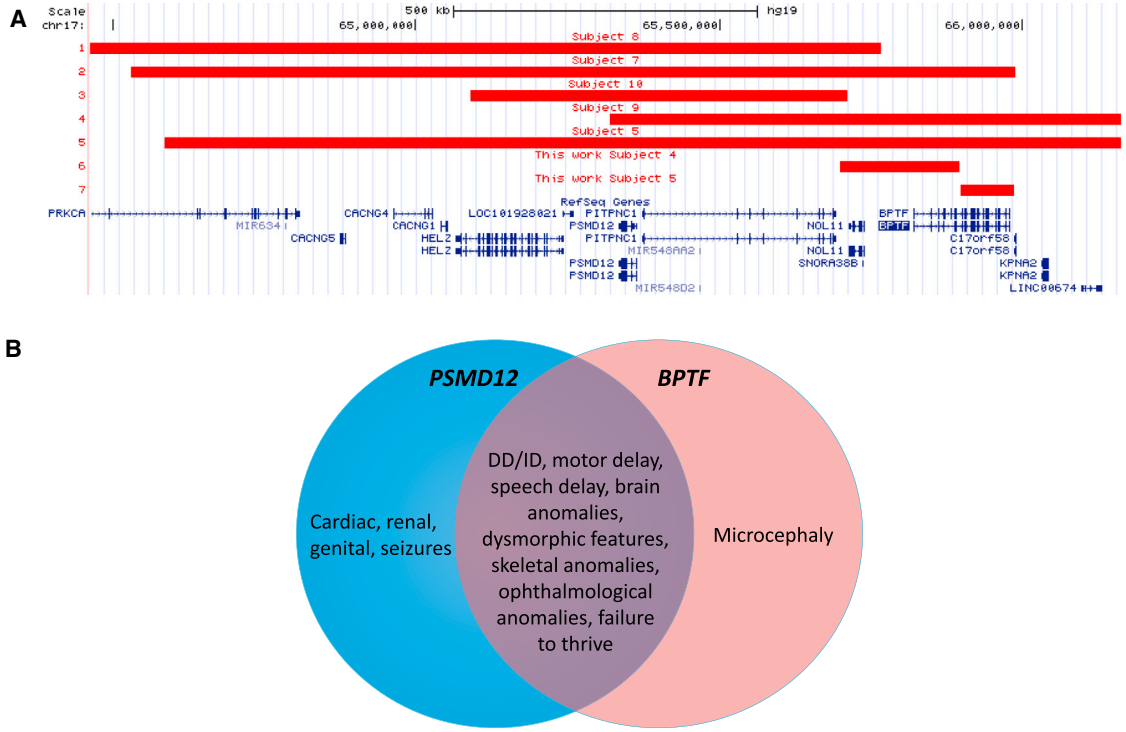

Figure 3. Analysis of the 17q24.2 Microdeletion Region
(A) Deletions in affected individuals reported previously[39] and in this study.
(B) Phenotype comparison of *PSMD12*-[39] and *BPTF*-related disorders. Individuals with deletions affecting both genes are expected to have blended phenotypes.

motor disabilities, epilepsy, and ophthalmological disorders.[56] No epilepsy was observed in our cohort. Brain anomalies detected in MRI include small anterior pituitary in subject 1, bilateral nonspecific multifocal white matter lesions in subject 2, pituitary hypoplasia in subject 7, reduced signal intensity of frontal and temporal white matter in subject 8, periventricular white matter lesions in subject 9, and borderline low-lying cerebellar tonsil on the right in subject 10. Ophthalmological abnormalities include: outward deviation of the eye (individual 1); left colobomatous (iris and disk) microphthalmia; slight inferior lens subluxation; telecanthus (individual 10); myopia (individuals 7 and 10); up-slanting or short palpebral fissures (individuals 4, 5 and 7, 8, respectively); and cataract and hyperopia (individual 9). The most characteristic facial feature observed is prominent nose (observed in subjects 2, 4, 6, 7–10). Other commonly shared features include toe/foot (subjects 2, 6, 7–9) and finger (subjects 2, 5–7, and 10) anomalies (Figure 1A, Table 1).

BPTF is located within the 17q24.2 microdeletion region, which encompasses multiple genes including *BPTF* and *PSMD12*. Recently, we have reported *de novo* disruption of the proteasome regulatory subunit *PSMD12* (MIM: 604450).[39] Reported subjects included four (individuals 1–4) with single-nucleotide variants in *PSMD12*, three (individuals 5, 7, and 9) with CNV deletions on 17q24.2 affecting *PSMD12*, *BPTF*, and other genes, and two (individuals 8 and 10) with deletions on 17q24.2 encompassing *PSMD12* and neighboring genes but leaving *BPTF* intact.[39] We hypothesize that the clinical phenotype of 17q24.2 microdeletion is associated with haploinsufficiency of the affected *PSMD12* and/or *BPTF*, and possibly additional genes. Within the reported deletion region on 17q24.2, five genes have pLI scores greater than 0.95 and are predicted to be highly intolerant of LoF mutations, including *PSMD12*, *BPTF*, and three other genes that are currently not implicated in disease: *HELZ*, *PITPNC1*, and *PRKCA* (Figure 3). The remaining protein-coding genes in this microdeletion region are predicted to be LoF tolerant. Comparison of the phenotypic features indicate that *PSMD12*- and *BPTF*-related disorders share clinical phenotypes including DD/ID, dysmorphisms, skeletal anomalies, and failure to thrive (Figure 3). The presence of cardiac, renal, genital, and ophthalmological defects and seizures were more commonly seen in individuals with *PSMD12* mutations while microcephaly was more commonly associated with a *BPTF* disruption. Notably, Küry et al.[39] also reported that individuals with 17q24.2 deletions involving *PSMD12* and *BPTF* had more prominent microcephaly than those with isolated *PSMD12* deficiency, supporting further the causative role of *BPTF* in microcephaly.

In addition to BPTF, there are more than 40 diverse proteins containing BRDs;[57] more than 20 of them display linked PHD fingers and BRDs.[58] Importantly, BRD-containing proteins have been implicated in numerous

developmental disorders,[59] e.g., *EP300* in Rubinstein-Taybi syndrome (RSTS2 [MIM: 613684]),[60] *BRWD3* (MRX93 [MIM: 300659]),[61] *WDR11* (HH14 [MIM: 614858]),[62] and *BRPF1* (IDDDFP [MIM: 617333]).[63] Moreover, genes encoding BRD-containing proteins have been also found mutated in multiple cancers.[57,64] For example, a number of them have been found at chromosomal translocation breakpoint fusions mapping at the BRDs and affecting their function,[57] e.g., *BRD4-NUT* fusion is detected in NUT midline carcinomas.[65] Notably, based on promising results in murine models, BRD proteins have become targets for drug development and translation.[66,67]

In aggregate, we propose that haploinsufficiency of *BPTF* results in an augmented neuronal death, which likely occurs mainly during the postnatal period and manifests with acquired microcephaly and neurodevelopmental abnormalities. Characteristic facial features involving nose and eyes as well as anomalies involving fingers and toes, resembling those reported in patients with 17q24.2 deletions,[68–72] enabled us to define a novel syndromic disorder. Genes encoding BRD and/or PHD represent strong candidates that could possibly contribute to human genetic disorders that involve a constellation of ID/DD, microcephaly, and dysmorphic features.

Accession Numbers

The accession numbers for the data reported in this paper are Leiden OpenVariation Database (LOVD) #00106517–00106527 and ClinVar SCV000584200–SCV000584209.

Supplemental Data

Supplemental Data include Supplemental Note, 3 figures, and 3 tables and can be found with this article online at http://dx.doi.org/10.1016/j.ajhg.2017.08.014.

Acknowledgments

We thank all families for participating in this study. We thank Mr. Z. Kupchinsky for zebrafish husbandry and automated imaging support. Evaluation of subject 3 was through support from U01HG006485 to S.E.P. The DDD study presents independent research commissioned by the Health Innovation Challenge Fund (grant number HICF-1009-003), a parallel funding partnership between the Wellcome Trust and the Department of Health, and the Wellcome Trust Sanger Institute (grant number WT098051). The views expressed in this publication are those of the author(s) and not necessarily those of the Wellcome Trust or the Department of Health. The research team acknowledges the support of the National Institute for Health Research, through the Comprehensive Clinical Research Network. This study makes use of data generated by the DECIPHER community. A full list of centers who contributed to the generation of the data is available from https://decipher.sanger.ac.uk and via email from decipher@sanger.ac.uk. Funding for the project was provided by the Wellcome Trust. E.E.D. is supported by US NIH grant R01 MH106826. The research team acknowledges the support of the National Institute for Health Research, through the Comprehensive Clinical Research Network. S.E.P. is a member of the Scientific Advisory Board (SAB) of Baylor Genetics Laboratories. A.R. is supported by CHROMATIN-Net funded by German Federal Ministry of Education and Research (BMBF, grant number 01GM1520A). N.K. is a paid consultant for and holds significant stock of Rescindo Therapeutics, Inc. Y.Y. is a member of the Scientific Advisory Board (SAB) of Veritas Genetics China. The Department of Molecular and Human Genetics at Baylor College of Medicine derives revenue from the chromosomal microarray analysis and clinical exome sequencing offered by Baylor Genetics.

Received: July 6, 2017
Accepted: August 10, 2017
Published: September 21, 2017

Web Resources

1000 Genomes, http://www.internationalgenome.org/
Baylor Genetics Laboratory, http://bmgl.com/
CHOPCHOP, http://chopchop.cbu.uib.no/
ClinVar, https://www.ncbi.nlm.nih.gov/clinvar/
Database of Genomic Variants (DGV), http://dgv.tcag.ca/dgv/app/home
dbSNP, https://www.ncbi.nlm.nih.gov/projects/SNP/
DECIPHER, https://decipher.sanger.ac.uk/
ExAC Browser, http://exac.broadinstitute.org/
GenBank, https://www.ncbi.nlm.nih.gov/genbank/
GeneMatcher, https://genematcher.org/
gnomAD Browser, http://gnomad.broadinstitute.org/
Human Splicing Finder, http://www.umd.be/HSF3/
LOVD, http://www.lovd.nl/3.0/home
MaxEntScan, http://genes.mit.edu/burgelab/maxent/Xmaxentscan_scoreseq.html
NHLBI Exome Sequencing Project (ESP) Exome Variant Server, http://evs.gs.washington.edu/EVS/
OMIM, http://www.omim.org/
Primer3, http://bioinfo.ut.ee/primer3
SPIDEX, http://tools.genes.toronto.edu/
SWISS-MODEL, http://swissmodel.expasy.org/
UCSC Genome Browser, http://genome.ucsc.edu

References

1. Bartholomew, B. (2014). Regulating the chromatin landscape: structural and mechanistic perspectives. Annu. Rev. Biochem. *83*, 671–696.
2. Badenhorst, P., Voas, M., Rebay, I., and Wu, C. (2002). Biological functions of the ISWI chromatin remodeling complex NURF. Genes Dev. *16*, 3186–3198.
3. Bai, X., Larschan, E., Kwon, S.Y., Badenhorst, P., and Kuroda, M.I. (2007). Regional control of chromatin organization by noncoding roX RNAs and the NURF remodeling complex in *Drosophila melanogaster*. Genetics *176*, 1491–1499.
4. Kwon, S.Y., Xiao, H., Glover, B.P., Tjian, R., Wu, C., and Badenhorst, P. (2008). The nucleosome remodeling factor (NURF) regulates genes involved in *Drosophila* innate immunity. Dev. Biol. *316*, 538–547.
5. Hamiche, A., Sandaltzopoulos, R., Gdula, D.A., and Wu, C. (1999). ATP-dependent histone octamer sliding mediated by the chromatin remodeling complex NURF. Cell *97*, 833–842.

6. Tsukiyama, T., and Wu, C. (1995). Purification and properties of an ATP-dependent nucleosome remodeling factor. Cell *83*, 1011–1020.
7. Alkhatib, S.G., and Landry, J.W. (2011). The nucleosome remodeling factor. FEBS Lett. *585*, 3197–3207.
8. Barak, O., Lazzaro, M.A., Lane, W.S., Speicher, D.W., Picketts, D.J., and Shiekhattar, R. (2003). Isolation of human NURF: a regulator of Engrailed gene expression. EMBO J. *22*, 6089–6100.
9. Xiao, H., Sandaltzopoulos, R., Wang, H.M., Hamiche, A., Ranallo, R., Lee, K.M., Fu, D., and Wu, C. (2001). Dual functions of largest NURF subunit NURF301 in nucleosome sliding and transcription factor interactions. Mol. Cell *8*, 531–543.
10. Jones, M.H., Hamana, N., and Shimane, M. (2000). Identification and characterization of BPTF, a novel bromodomain transcription factor. Genomics *63*, 35–39.
11. Filippakopoulos, P., Picaud, S., Mangos, M., Keates, T., Lambert, J.P., Barsyte-Lovejoy, D., Felletar, I., Volkmer, R., Müller, S., Pawson, T., et al. (2012). Histone recognition and large-scale structural analysis of the human bromodomain family. Cell *149*, 214–231.
12. Li, H., Ilin, S., Wang, W., Duncan, E.M., Wysocka, J., Allis, C.D., and Patel, D.J. (2006). Molecular basis for site-specific read-out of histone H3K4me3 by the BPTF PHD finger of NURF. Nature *442*, 91–95.
13. Ruthenburg, A.J., Li, H., Milne, T.A., Dewell, S., McGinty, R.K., Yuen, M., Ueberheide, B., Dou, Y., Muir, T.W., Patel, D.J., and Allis, C.D. (2011). Recognition of a mononucleosomal histone modification pattern by BPTF via multivalent interactions. Cell *145*, 692–706.
14. Wysocka, J., Swigut, T., Xiao, H., Milne, T.A., Kwon, S.Y., Landry, J., Kauer, M., Tackett, A.J., Chait, B.T., Badenhorst, P., et al. (2006). A PHD finger of NURF couples histone H3 lysine 4 trimethylation with chromatin remodelling. Nature *442*, 86–90.
15. Goller, T., Vauti, F., Ramasamy, S., and Arnold, H.H. (2008). Transcriptional regulator BPTF/FAC1 is essential for trophoblast differentiation during early mouse development. Mol. Cell. Biol. *28*, 6819–6827.
16. Landry, J., Sharov, A.A., Piao, Y., Sharova, L.V., Xiao, H., Southon, E., Matta, J., Tessarollo, L., Zhang, Y.E., Ko, M.S., et al. (2008). Essential role of chromatin remodeling protein Bptf in early mouse embryos and embryonic stem cells. PLoS Genet. *4*, e1000241.
17. Mayes, K., Alkhatib, S.G., Peterson, K., Alhazmi, A., Song, C., Chan, V., Blevins, T., Roberts, M., Dumur, C.I., Wang, X.Y., and Landry, J.W. (2016). BPTF depletion enhances T-cell-mediated antitumor immunity. Cancer Res. *76*, 6183–6192.
18. Ma, Y., Liu, X., Liu, Z., Wei, S., Shang, H., Xue, Y., Cao, Y., Meng, A., and Wang, Q. (2015). The chromatin remodeling protein Bptf promotes posterior neuroectodermal fate by enhancing Smad2-activated wnt8a expression. J. Neurosci. *35*, 8493–8506.
19. Dobolyi, A., Vincze, C., Pál, G., and Lovas, G. (2012). The neuroprotective functions of transforming growth factor beta proteins. Int. J. Mol. Sci. *13*, 8219–8258.
20. Erter, C.E., Wilm, T.P., Basler, N., Wright, C.V., and Solnica-Krezel, L. (2001). Wnt8 is required in lateral mesendodermal precursors for neural posteriorization in vivo. Development *128*, 3571–3583.
21. Buganim, Y., Goldstein, I., Lipson, D., Milyavsky, M., Polak-Charcon, S., Mardoukh, C., Solomon, H., Kalo, E., Madar, S., Brosh, R., et al. (2010). A novel translocation breakpoint within the BPTF gene is associated with a pre-malignant phenotype. PLoS ONE *5*, e9657.
22. Dai, M., Lu, J.J., Guo, W., Yu, W., Wang, Q., Tang, R., Tang, Z., Xiao, Y., Li, Z., Sun, W., et al. (2015). BPTF promotes tumor growth and predicts poor prognosis in lung adenocarcinomas. Oncotarget *6*, 33878–33892.
23. Gong, Y.C., Liu, D.C., Li, X.P., and Dai, S.P. (2017). BPTF biomarker correlates with poor survival in human NSCLC. Eur. Rev. Med. Pharmacol. Sci. *21*, 102–107.
24. Lee, J.H., Kim, M.S., Yoo, N.J., and Lee, S.H. (2016). BPTF, a chromatin remodeling-related gene, exhibits frameshift mutations in gastric and colorectal cancers. APMIS *124*, 425–427.
25. Richart, L., Carrillo-de Santa Pau, E., Río-Machín, A., de Andrés, M.P., Cigudosa, J.C., Lobo, V.J., and Real, F.X. (2016). BPTF is required for c-MYC transcriptional activity and in vivo tumorigenesis. Nat. Commun. *7*, 10153.
26. Xiao, S., Liu, L., Fang, M., Zhou, X., Peng, X., Long, J., and Lu, X. (2015). BPTF associated with EMT indicates negative prognosis in patients with hepatocellular carcinoma. Dig. Dis. Sci. *60*, 910–918.
27. Wu, B., Wang, Y., Wang, C., Wang, G.G., Wu, J., and Wan, Y.Y. (2016). BPTF is essential for T cell homeostasis and function. J. Immunol. *197*, 4325–4333.
28. Mayes, K., Elsayed, Z., Alhazmi, A., Waters, M., Alkhatib, S.G., Roberts, M., Song, C., Peterson, K., Chan, V., Ailaney, N., et al. (2017). BPTF inhibits NK cell activity and the abundance of natural cytotoxicity receptor co-ligands. Oncotarget. http://dx.doi.org/10.18632/oncotarget.17834.
29. Frey, W.D., Chaudhry, A., Slepicka, P.F., Ouellette, A.M., Kirberger, S.E., Pomerantz, W.C.K., Hannon, G.J., and Dos Santos, C.O. (2017). BPTF maintains chromatin accessibility and the self-renewal capacity of mammary gland stem cells. Stem Cell Reports *9*, 23–31.
30. Firth, H.V., Richards, S.M., Bevan, A.P., Clayton, S., Corpas, M., Rajan, D., Van Vooren, S., Moreau, Y., Pettett, R.M., and Carter, N.P. (2009). DECIPHER: Database of Chromosomal Imbalance and Phenotype in Humans Using Ensembl Resources. Am. J. Hum. Genet. *84*, 524–533.
31. Deciphering Developmental Disorders Study (2015). Large-scale discovery of novel genetic causes of developmental disorders. Nature *519*, 223–228.
32. Sobreira, N., Schiettecatte, F., Valle, D., and Hamosh, A. (2015). GeneMatcher: a matching tool for connecting investigators with an interest in the same gene. Hum. Mutat. *36*, 928–930.
33. Yang, Y., Muzny, D.M., Xia, F., Niu, Z., Person, R., Ding, Y., Ward, P., Braxton, A., Wang, M., Buhay, C., et al. (2014). Molecular findings among patients referred for clinical whole-exome sequencing. JAMA *312*, 1870–1879.
34. Boone, P.M., Bacino, C.A., Shaw, C.A., Eng, P.A., Hixson, P.M., Pursley, A.N., Kang, S.H., Yang, Y., Wiszniewska, J., Nowakowska, B.A., et al. (2010). Detection of clinically relevant exonic copy-number changes by array CGH. Hum. Mutat. *31*, 1326–1342.
35. Wiszniewska, J., Bi, W., Shaw, C., Stankiewicz, P., Kang, S.H., Pursley, A.N., Lalani, S., Hixson, P., Gambin, T., Tsai, C.H., et al. (2014). Combined array CGH plus SNP genome analyses in a single assay for optimized clinical testing. Eur. J. Hum. Genet. *22*, 79–87.

36. Farwell, K.D., Shahmirzadi, L., El-Khechen, D., Powis, Z., Chao, E.C., Tippin Davis, B., Baxter, R.M., Zeng, W., Mroske, C., Parra, M.C., et al. (2015). Enhanced utility of family-centered diagnostic exome sequencing with inheritance model-based analysis: results from 500 unselected families with undiagnosed genetic conditions. Genet. Med. *17*, 578–586.
37. Farwell Hagman, K.D., Shinde, D.N., Mroske, C., Smith, E., Radtke, K., Shahmirzadi, L., El-Khechen, D., Powis, Z., Chao, E.C., Alcaraz, W.A., et al. (2017). Candidate-gene criteria for clinical reporting: diagnostic exome sequencing identifies altered candidate genes among 8% of patients with undiagnosed diseases. Genet. Med. *19*, 224–235.
38. Montague, T.G., Cruz, J.M., Gagnon, J.A., Church, G.M., and Valen, E. (2014). CHOPCHOP: a CRISPR/Cas9 and TALEN web tool for genome editing. Nucleic Acids Res. *42*, W401–W407.
39. Küry, S., Besnard, T., Ebstein, F., Khan, T.N., Gambin, T., Douglas, J., Bacino, C.A., Craigen, W.J., Sanders, S.J., Lehmann, A., et al. (2017). De novo disruption of the proteasome regulatory subunit PSMD12 causes a syndromic neurodevelopmental disorder. Am. J. Hum. Genet. *100*, 352–363.
40. Zhu, X., Xu, Y., Yu, S., Lu, L., Ding, M., Cheng, J., Song, G., Gao, X., Yao, L., Fan, D., et al. (2014). An efficient genotyping method for genome-modified animals and human cells generated with CRISPR/Cas9 system. Sci. Rep. *4*, 6420.
41. Kague, E., Gallagher, M., Burke, S., Parsons, M., Franz-Odendaal, T., and Fisher, S. (2012). Skeletogenic fate of zebrafish cranial and trunk neural crest. PLoS ONE *7*, e47394.
42. Isrie, M., Breuss, M., Tian, G., Hansen, A.H., Cristofoli, F., Morandell, J., Kupchinsky, Z.A., Sifrim, A., Rodriguez-Rodriguez, C.M., Dapena, E.P., et al. (2015). Mutations in either TUBB or MAPRE2 cause circumferential skin creases Kunze type. Am. J. Hum. Genet. *97*, 790–800.
43. Golzio, C., Willer, J., Talkowski, M.E., Oh, E.C., Taniguchi, Y., Jacquemont, S., Reymond, A., Sun, M., Sawa, A., Gusella, J.F., et al. (2012). KCTD13 is a major driver of mirrored neuroanatomical phenotypes of the 16p11.2 copy number variant. Nature *485*, 363–367.
44. Parsons, D.W., Roy, A., Yang, Y., Wang, T., Scollon, S., Bergstrom, K., Kerstein, R.A., Gutierrez, S., Petersen, A.K., Bavle, A., et al. (2016). Diagnostic Yield of Clinical Tumor and Germline Whole-Exome Sequencing for Children With Solid Tumors. JAMA Oncol. Published online January 28, 2016. http://dx.doi.org/10.1001/jamaoncol.2015.5699.
45. Kim, H.T., Lee, M.S., Choi, J.H., Jung, J.Y., Ahn, D.G., Yeo, S.Y., Choi, D.K., and Kim, C.H. (2011). The microcephaly gene aspm is involved in brain development in zebrafish. Biochem. Biophys. Res. Commun. *409*, 640–644.
46. Nakayama, T., Al-Maawali, A., El-Quessny, M., Rajab, A., Khalil, S., Stoler, J.M., Tan, W.H., Nasir, R., Schmitz-Abe, K., Hill, R.S., et al. (2015). Mutations in PYCR2, encoding pyrroline-5-carboxylate reductase 2, cause microcephaly and hypomyelination. Am. J. Hum. Genet. *96*, 709–719.
47. Ta-Shma, A., Khan, T.N., Vivante, A., Willer, J.R., Matak, P., Jalas, C., Pode-Shakked, B., Salem, Y., Anikster, Y., Hildebrandt, F., et al. (2017). Mutations in TMEM260 cause a pediatric neurodevelopmental, cardiac, and renal syndrome. Am. J. Hum. Genet. *100*, 666–675.
48. Bohnsack, B.L., Kasprick, D.S., Kish, P.E., Goldman, D., and Kahana, A. (2012). A zebrafish model of axenfeld-rieger syndrome reveals that pitx2 regulation by retinoic acid is essential for ocular and craniofacial development. Invest. Ophthalmol. Vis. Sci. *53*, 7–22.
49. Dauber, A., Golzio, C., Guenot, C., Jodelka, F.M., Kibaek, M., Kjaergaard, S., Leheup, B., Martinet, D., Nowaczyk, M.J., Rosenfeld, J.A., et al. (2013). SCRIB and PUF60 are primary drivers of the multisystemic phenotypes of the 8q24.3 copy-number variant. Am. J. Hum. Genet. *93*, 798–811.
50. Frosk, P., Arts, H.H., Philippe, J., Gunn, C.S., Brown, E.L., Chodirker, B., Simard, L., Majewski, J., Fahiminiya, S., Russell, C., et al.; FORGE Canada Consortium; and Canadian Rare Diseases: Models & Mechanisms Network (2017). A truncating mutation in CEP55 is the likely cause of MARCH, a novel syndrome affecting neuronal mitosis. J. Med. Genet. *54*, 490–501.
51. Gordon, C.T., Weaver, K.N., Zechi-Ceide, R.M., Madsen, E.C., Tavares, A.L., Oufadem, M., Kurihara, Y., Adameyko, I., Picard, A., Breton, S., et al. (2015). Mutations in the endothelin receptor type A cause mandibulofacial dysostosis with alopecia. Am. J. Hum. Genet. *96*, 519–531.
52. Shaw, N.D., Brand, H., Kupchinsky, Z.A., Bengani, H., Plummer, L., Jones, T.I., Erdin, S., Williamson, K.A., Rainger, J., Stortchevoi, A., et al. (2017). SMCHD1 mutations associated with a rare muscular dystrophy can also cause isolated arhinia and Bosma arhinia microphthalmia syndrome. Nat. Genet. *49*, 238–248.
53. Lek, M., Karczewski, K.J., Minikel, E.V., Samocha, K.E., Banks, E., Fennell, T., O'Donnell-Luria, A.H., Ware, J.S., Hill, A.J., Cummings, B.B., et al.; Exome Aggregation Consortium (2016). Analysis of protein-coding genetic variation in 60,706 humans. Nature *536*, 285–291.
54. Seltzer, L.E., and Paciorkowski, A.R. (2014). Genetic disorders associated with postnatal microcephaly. Am. J. Med. Genet. C. Semin. Med. Genet. *166C*, 140–155.
55. Woods, C.G. (2004). Human microcephaly. Curr. Opin. Neurobiol. *14*, 112–117.
56. von der Hagen, M., Pivarcsi, M., Liebe, J., von Bernuth, H., Didonato, N., Hennermann, J.B., Bührer, C., Wieczorek, D., and Kaindl, A.M. (2014). Diagnostic approach to microcephaly in childhood: a two-center study and review of the literature. Dev. Med. Child Neurol. *56*, 732–741.
57. Fujisawa, T., and Filippakopoulos, P. (2017). Functions of bromodomain-containing proteins and their roles in homeostasis and cancer. Nat. Rev. Mol. Cell Biol. *18*, 246–262.
58. Ruthenburg, A.J., Li, H., Patel, D.J., and Allis, C.D. (2007). Multivalent engagement of chromatin modifications by linked binding modules. Nat. Rev. Mol. Cell Biol. *8*, 983–994.
59. Li, J., Zhao, G., and Gao, X. (2013). Development of neurodevelopmental disorders: a regulatory mechanism involving bromodomain-containing proteins. J. Neurodev. Disord. *5*, 4.
60. Roelfsema, J.H., White, S.J., Ariyürek, Y., Bartholdi, D., Niedrist, D., Papadia, F., Bacino, C.A., den Dunnen, J.T., van Ommen, G.J., Breuning, M.H., et al. (2005). Genetic heterogeneity in Rubinstein-Taybi syndrome: mutations in both the CBP and EP300 genes cause disease. Am. J. Hum. Genet. *76*, 572–580.
61. Field, M., Tarpey, P.S., Smith, R., Edkins, S., O'Meara, S., Stevens, C., Tofts, C., Teague, J., Butler, A., Dicks, E., et al. (2007). Mutations in the BRWD3 gene cause X-linked mental retardation associated with macrocephaly. Am. J. Hum. Genet. *81*, 367–374.
62. Kim, H.G., Ahn, J.W., Kurth, I., Ullmann, R., Kim, H.T., Kulharya, A., Ha, K.S., Itokawa, Y., Meliciani, I., Wenzel, W., et al. (2010). WDR11, a WD protein that interacts with transcription factor EMX1, is mutated in idiopathic

hypogonadotropic hypogonadism and Kallmann syndrome. Am. J. Hum. Genet. *87*, 465–479.

63. Yan, K., Rousseau, J., Littlejohn, R.O., Kiss, C., Lehman, A., Rosenfeld, J.A., Stumpel, C.T., Stegmann, A.P., Robak, L., Scaglia, F., et al.; DDD Study; and CAUSES Study (2017). Mutations in the chromatin regulator gene BRPF1 cause syndromic intellectual disability and deficient histone acetylation. Am. J. Hum. Genet. *100*, 91–104.
64. Huether, R., Dong, L., Chen, X., Wu, G., Parker, M., Wei, L., Ma, J., Edmonson, M.N., Hedlund, E.K., Rusch, M.C., et al. (2014). The landscape of somatic mutations in epigenetic regulators across 1,000 paediatric cancer genomes. Nat. Commun. *5*, 3630.
65. French, C.A., Miyoshi, I., Kubonishi, I., Grier, H.E., Perez-Atayde, A.R., and Fletcher, J.A. (2003). BRD4-NUT fusion oncogene: a novel mechanism in aggressive carcinoma. Cancer Res. *63*, 304–307.
66. Filippakopoulos, P., Qi, J., Picaud, S., Shen, Y., Smith, W.B., Fedorov, O., Morse, E.M., Keates, T., Hickman, T.T., Felletar, I., et al. (2010). Selective inhibition of BET bromodomains. Nature *468*, 1067–1073.
67. Wang, C.Y., and Filippakopoulos, P. (2015). Beating the odds: BETs in disease. Trends Biochem. Sci. *40*, 468–479.
68. Naud, M.E., Tosca, L., Martinovic, J., Saada, J., Métay, C., Drévillon, L., Benoit, V., Brisset, S., and Tachdjian, G. (2017). Prenatal diagnosis of a 2.5 Mb de novo 17q24.1q24.2 deletion encompassing *KPNA2* and *PSMD12* genes in a fetus with craniofacial dysmorphism, equinovarus feet, and syndactyly. Case Rep. Genet. *2017*, 7803136.
69. Stewart, D.R., Pemov, A., Johnston, J.J., Sapp, J.C., Yeager, M., He, J., Boland, J.F., Burdett, L., Brown, C., Gatti, R.A., et al. (2014). Dubowitz syndrome is a complex comprised of multiple, genetically distinct and phenotypically overlapping disorders. PLoS ONE *9*, e98686.
70. Bartnik, M., Nowakowska, B., Derwińska, K., Wiśniowiecka-Kowalnik, B., Kędzior, M., Bernaciak, J., Ziemkiewicz, K., Gambin, T., Sykulski, M., Bezniakow, N., et al. (2014). Application of array comparative genomic hybridization in 256 patients with developmental delay or intellectual disability. J. Appl. Genet. *55*, 125–144.
71. Vergult, S., Dauber, A., Delle Chiaie, B., Van Oudenhove, E., Simon, M., Rihani, A., Loeys, B., Hirschhorn, J., Pfotenhauer, J., Phillips, J.A., 3rd., et al. (2012). 17q24.2 microdeletions: a new syndromal entity with intellectual disability, truncal obesity, mood swings and hallucinations. Eur. J. Hum. Genet. *20*, 534–539.
72. Blyth, M., Huang, S., Maloney, V., Crolla, J.A., and Karen Temple, I. (2008). A 2.3 Mb deletion of 17q24.2-q24.3 associated with 'Carney Complex plus'. Eur. J. Med. Genet. *51*, 672–678.

The American Journal of Human Genetics, Volume *101*

Supplemental Data

Haploinsufficiency of the Chromatin Remodeler *BPTF* Causes Syndromic Developmental and Speech Delay, Postnatal Microcephaly, and Dysmorphic Features

Paweł Stankiewicz, Tahir N. Khan, Przemyslaw Szafranski, Leah Slattery, Haley Streff, Francesco Vetrini, Jonathan A. Bernstein, Chester W. Brown, Jill A. Rosenfeld, Surya Rednam, Sarah Scollon, Katie L. Bergstrom, Donald W. Parsons, Sharon E. Plon, Marta W. Vieira, Caio R.D.C. Quaio, Wagner A.R. Baratela, Johanna C. Acosta Guio, Ruth Armstrong, Sarju G. Mehta, Patrick Rump, Rolph Pfundt, Raymond Lewandowski, Erica M. Fernandes, Deepali N. Shinde, Sha Tang, Juliane Hoyer, Christiane Zweier, André Reis, Carlos A. Bacino, Rui Xiao, Amy M. Breman, Janice L. Smith, Deciphering Developmental Disorders Study, Nicholas Katsanis, Bret Bostwick, Bernt Popp, Erica E. Davis, and Yaping Yang

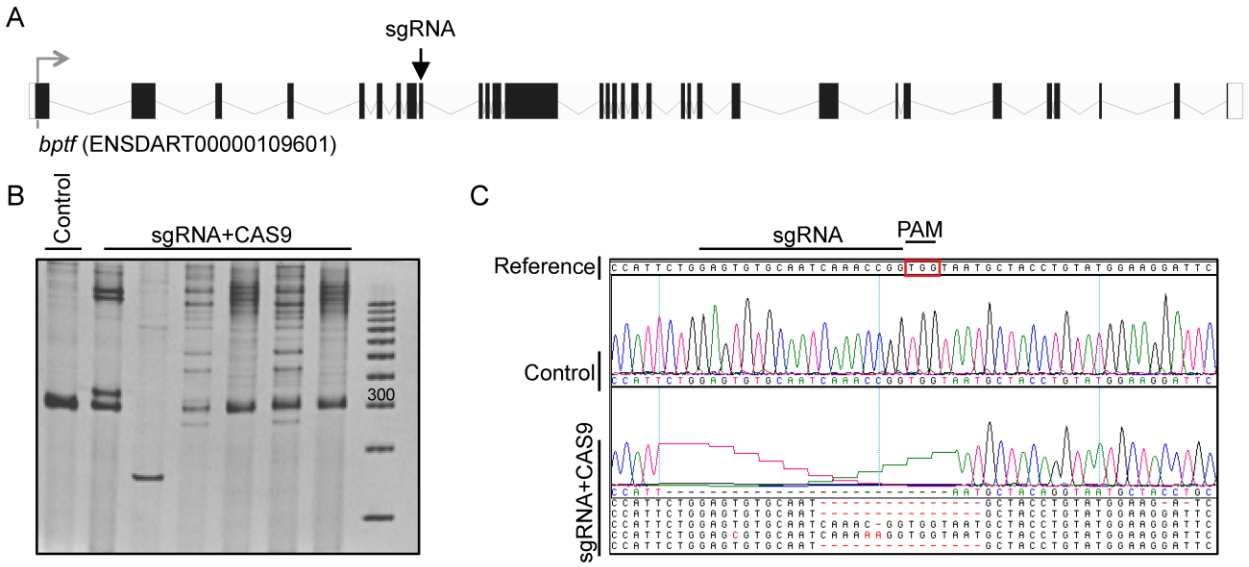

Figure S1. CRISPR/CAS9 genome editing efficiency of the *bptf* locus

(A) Schematic of *D. rerio bptf* showing the exon-intron structure of the gene; blue boxes coding exons, white boxes; untranslated regions, connecting lines; introns. The position of the CRISPR sgRNA is denoted with an arrow. (B) Polyacrylamide gel electrophoresis (15% PAGE; BioRad) shows the presence of heteroduplexes indicating targeting events in one control and six individual F0 embryos injected with sgRNA and CAS9 protein and harvested for DNA extraction at 2 days post-fertilization. (C) Representative chromatograms corresponding to cloned PCR products flanking the sgRNA target site amplified from uninjected control embryos and F0 embryos show mutational events in the target region compared to uninjected control embryo. (PAM; protospacer adjacent motif; enclosed in red rectangle).

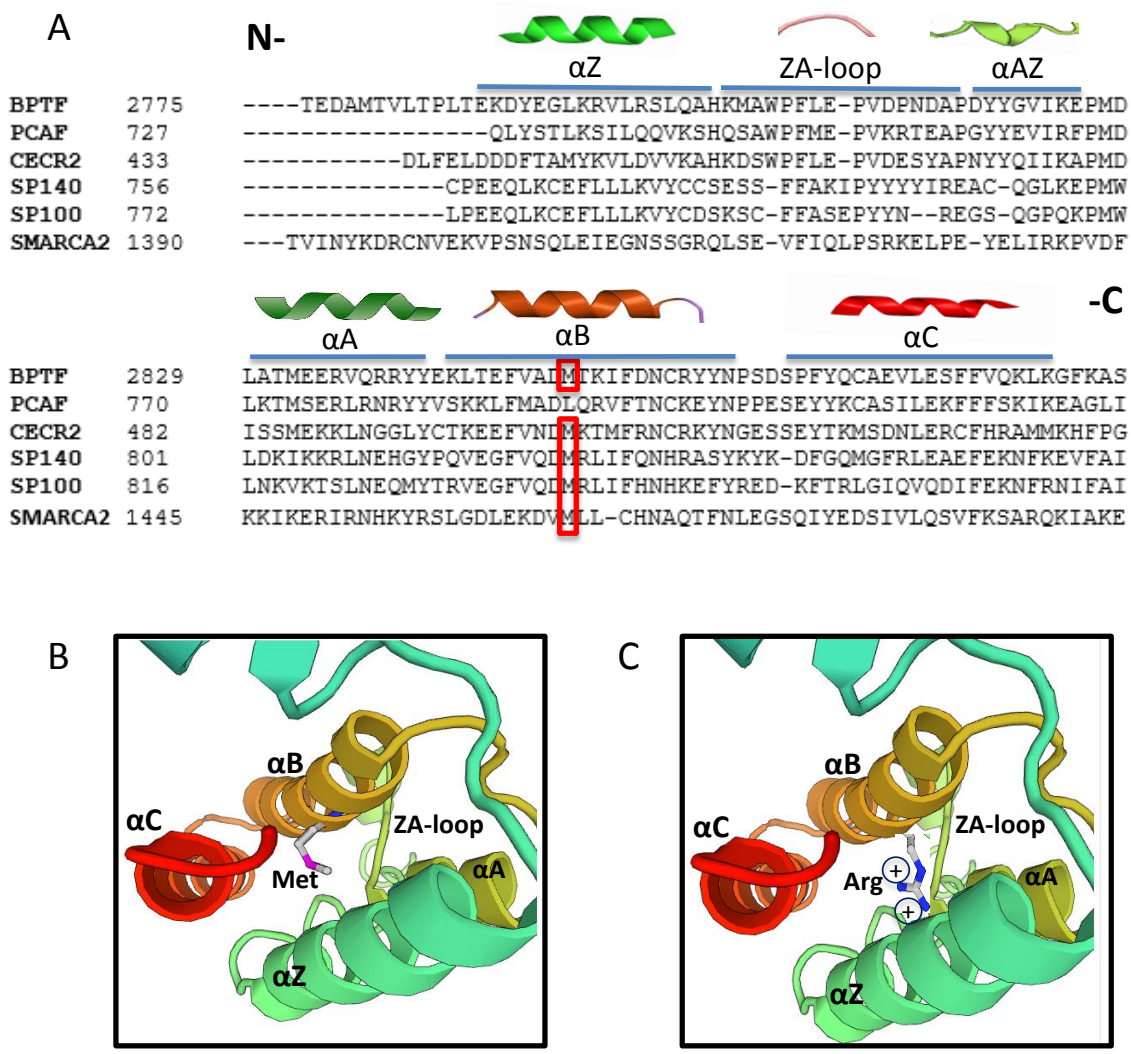

Figure S2. Potential consequences of the p.Met2853Arg substitution on the stability of the hydrophobic four α-helices bundle pocket of the BPTF bromodomain

(A) ClustalW sequence alignment of the bromodomain motifs of a selected number of human bromodomain-containing proteins; the relative starting positions are numbered; -N=N-terminal, -C=C-terminal. The regions corresponding to the four α-helices and variable loop regions are indicated by ribbons and defined by a blue line according to previous structural studies.[1,2] The highly conserved Met including Met2853 of BPTF protein are boxed in red. (B) 3D simulation based on crystal structure of PHD finger-linker-bromodomain fragment of human BPTF (PDB_id:3UV2) obtained with Swiss-Model bioinformatic tool (http://swissmodel.expasy.org/)[3] showing the characteristic conserved hydrophobic core of the four α-helices bundle; Met2853 is shown protruding from the αB helix into the hydrophobic pocket. (C) The effect of the substitution of Met at the position 2853 with the positively charged Arg in the hydrophobic core may destabilize the 3D conformation of the bromodomain and ultimately interfere with its activity.

Subject 4

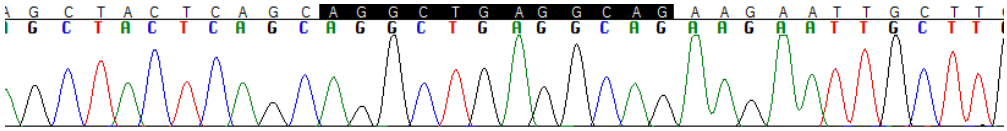

Subject 5

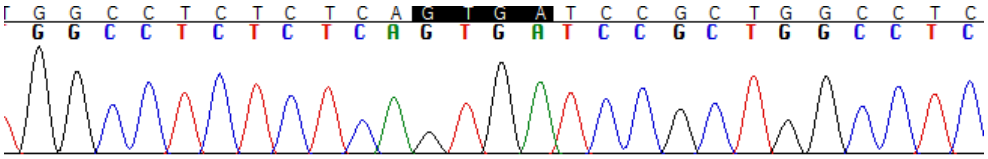

Figure S3: **Chromatograms showing results of Sanger sequencing of breakpoint in CNV deletions identified in Subjects 4 and 5**

In subject 4, the proximal deletion breakpoint was mapped within in *Alu*Sx between chr17:65,700,189-65,700,200 and the distal breakpoint within *Alu*Sz6 between chr17:65,896,331-65,896,342 with 12 bp microhomology. In subject 5, the proximal deletion breakpoint was mapped within a unique sequence between chr17:65,898,399-65,898,404 and the distal breakpoint within *Alu*Sp between 65,986,981-65,986,986 with a 4 bp GTGA microhomology.

Table S1. Additional clinical findings in individuals with *BPTF* variants.

	Subject 1	Subject 2	Subject 3	Subject 4	Subject 5	Subject 6	Subject 7	Subject 8	Subject 9	Subject 10
Other abnormalities	Unilateral choanal atresia, constipation, failure to thrive, patent ductus arteriosus	Dental caries	Pheochromocytoma associated with *VHL* (pathogenic variant)	De novo 1 kb CNV deletion in 14q11.2 (chr14:21,681,066-21,682,235) (variant of unknown significance)	FTT, 703 kb CNV duplication in 2q12.3 (chr2108,403,191-109,106,402) (likely benign variant)	Autistic spectrum disorder, unusual mannerisms – hand flapping, jumping	Constantly busy, chronic diarrhea; borderline thyroid function, hypermobility, pituitary hypoplasia with growth hormone deficiency, pancreatic insufficiency, low pitched voice, lack of subcutaneous fat	FTT, feeding problems with g-tube dependence	Elevated first-trimester nuchal translucency erythema toxicum neonatoru, membrana pupillaris persistens, bilateral maldescensed testes, frequent infections and diarrhea with vomiting as an infant, FTT, dyslalia, dysgrammatism, good speech comprehension, delayed motor skills, ataxia	FTT with g-tube dependence, pain amplification syndrome, GI dysmotility, chronic headaches, pain amplification syndrome

FTT, failure to thrive

Table S2. Prediction Effect of Missense Mutations in Affected Individuals

ID	Subject 7	Subject 8
CHROM	chr17:g.65914918G>A	chr17:65971957T>G
GENE	*BPTF*	*BPTF*
FEATUREID	NM_004459.6	NM_004459.6
EFFECT	Missense variant	Missense variant
IMPACT	MODERATE	MODERATE
HGVS_C	c.5770G>A	c.8558T>G
HGVS_P	p.Ala1924Thr	p.Met2853Arg
ExAC31_AC	0	0
dbNSFP_CADD_phred	26.7	29.0
dbNSFP_M-CAP_score	0.0118444082406	0.108952265306
REVEL_score	0.247	0.513
dbNSFP_SIFT_score	0.118	0.0
dbNSFP_Polyphen2_HVAR_score	0.995	0.963
dbNSFP_MutationTaster_score	0.999988	1.0
spidex_dpsi_zscore	0.91	-1.349

Method Authors' recommended threshold: CADD >20, M-CAP <0.025, REVEL >0.5, SIFT <0.05, PolyPhen-2 >0.8, spidex_dpsi_zscore <-2.0, dbscSNV_ada_score >0.6, dbscSNV_rf_score >0.6

Table S3. Oligos for CRISPR sgRNA design and target amplification

bptf_sgRNA_F	5'-TAATACGACTCACTATAG*GAGTGTGCAATCAAACCGG*-3'
bptf_sgRNA_R	5'-TTCTAGCTCTAAAAC*CCGGTTTGATTGCACACTC*-3'
bptf_sgRNA_PCR_F	5'-TGCTCCATTCTTGCATCCCA-3'
bptf_sgRNA_PCR_R	5'-TGCATCAAACTTTGAGTTGTGCT'3-

sgRNA target sequence is shown in italics.

References

1. Filippakopoulos, P., Picaud, S., Mangos, M., Keates, T., Lambert, J.P., Barsyte-Lovejoy, D., Felletar, I., Volkmer, R., Muller, S., Pawson, T., et al. (2012). Histone recognition and large-scale structural analysis of the human bromodomain family. Cell 149, 214-231.
2. Zeng, L., and Zhou, M.M. (2002). Bromodomain: an acetyl-lysine binding domain. FEBS Lett 513, 124-128.3. Biasini, M., Bienert, S., Waterhouse, A., Konstantin, A., Studer, G., Schmidt, T., Kiefer, F., Gallo Cassarino, T., Bertoni M., et al. (2014). SWISS-MODEL: modeling protein tertiary and quaternary structure using evolutionary information. Nucleic Acids Res. 42, 252-258.

Acknowledgments

We thank Drs. B. Isidor, S. Küry, and A. Midro for helpful discussion. The views expressed in this publication are those of the author(s) and not necessarily those of the Wellcome Trust or the Department of Health.